JST: Smart Systems and Devices
Volume 35, Issue 3, September 2025, 034-044

Research on Modeling and Optimization for Surface Roughness of Al6061 Spherical in Ultra-Precision Turning Based on Neural Network and Bee Colony Optimization Algorithm

Hoang Nghia Duc [1], Duong Xuan Bien [1*], Bui Kim Hoa[1], Nguyen Kim Hung [1], Do Manh Tung[2], Ngo Viet Hung[1], Truong Khanh Nghia[3]

[1]*Center of Technology, University of Le Quy Don, Ha Noi, Vietnam*
[2] *Faculty of Mechanical Engineering, University of Le Quy Don, Ha Noi, Vietnam*
[3]*Institute of Simulation Technology, University of Le Quy Don, Ha Noi, Vietnam*
[*]*Corresponding author email: duongxuanbien@lqdtu.edu.vn*

Abstract

The article focuses on developing a predictive and optimization model for surface roughness in ultra-precision turning (UPT) using a diamond cutter on the spherical surface of Al6061 material. An experimental model with 30 experiments was established, considering three input parameters: spindle speed, feed rate, and depth of cut. The results from this model were collected to create an input dataset for an artificial neural network (ANN) to build a surface roughness prediction model. The ANN structure 3-5-10-1 provided the best prediction results, with Coefficient of Determination (R^2) is 0.98, Mean Absolute Percent Error ($MAPE$) is 13.36%, Mean Square Error (MSE) is 0.68, and Root Mean Square Error ($RMSE$) is 0.82. Additionally, the artificial bee colony (ABC) algorithm was employed to determine the optimal cutting parameters that minimize surface roughness. The results indicated that the minimum roughness value achieved was 0.76 nm with the cutting parameters: spindle speed of 823 rev/min, feed rate of 13 mm/min, and depth of cut of 1 µm. Moreover, the effects of different cutting parameter combinations on surface roughness were analyzed and evaluated. The integration of the ANN model with the ABC algorithm enables a reliable prediction model for surface roughness and demonstrates high efficiency in optimizing the objective function. This research contributes valuable insights into surface roughness prediction and optimization in ultra-precision turning of Al6061 material. Furthermore, the proposed modeling and optimization approach can be extended to other materials and the processing of aspherical and diffractive surfaces.

Keywords: ABC, ANN, surface roughness, ultra-precision turning, spherical.

1. Introduction

Ultra-precision machining (UPM) is becoming increasingly important due to its capability to fabricate ultra-small components with form accuracy below 0.2 µm and surface roughness under 10 nm. It is widely applied and indispensable in various high-tech industries such as optics, electronics, and semiconductors [1]. Among UPM techniques, Single Point Diamond Turning (SPDT) is commonly used for machining high-precision and complex-profile surfaces to meet the ever-growing demands in precision component manufacturing. SPDT enables the achievement of the desired surface finish on flat, spherical, and aspherical surfaces of lens mold components and mirror surfaces in optical systems [2]. Huang [3] explored the tool-material interaction mechanism in SPDT of single-crystal SiC, providing insights into the challenges and advantages of UPM in generating curved microstructures.

Spherical mirror surfaces play a crucial role in optical systems such as telescopes [4], optical metrology [5], and the fabrication of polymer mold negatives and positives for contact lenses and intraocular lenses [6]. These surfaces are typically manufactured using UPM techniques with materials such as ceramics, copper, and aluminum, particularly Aluminum 6061, which is widely used due to its machinability and ability to achieve high surface quality. Mukaida [7] presented the integration of SPDT with a slow tool servo (STS) system to generate single-crystal silicon spherical surfaces with low roughness and uniform structure, making them suitable for optical applications. The study also highlighted the influence of cutting parameters on spherical surface quality and proposed solutions to minimize tool wear during machining.

Surface roughness significantly affects the quality of optical systems as it causes scattering, reducing contrast, and the sharpness of optical images [8]. Numerous studies have highlighted the importance of controlling surface roughness in UPM. For instance, Zhang [9] comprehensively reviewed the factors

ISSN 2734-9373
https://doi.org/10.51316/jst.184.ssad.2025.35.3.5
Received: Feb 28, 2024; revised: Mar 30, 2025;
accepted: Apr 16, 2025

influencing surface roughness in UPM, including machine tool characteristics, cutting conditions, tool geometry, environmental conditions, material properties, chip formation, tool wear, and vibrations. Hatefi [10] provided an overview of SPDT, particularly emphasizing its capability to generate ultra-precision optical surfaces with extremely low roughness while analyzing the key factors affecting surface quality. Li [11] focused on analyzing the impact of low feed rate SPDT on the surface roughness and optical reflectivity of Al6061 aluminum alloy.

Optimizing surface roughness is essential for improving functional properties. For mold surfaces, it enhances the surface quality of molded products, while for mirror surfaces, it reduces light scattering and increases reflectivity. Gao [12] investigated the effects of cutting parameters on surface roughness in UPM, highlighting that process optimization can significantly improve surface quality. Similarly, Bensingh [13] optimized the injection molding process for double-spherical lenses, proving the feasibility of optimization techniques in improving surface finish.

According to Mozammel [14], among various artificial intelligence-based computational techniques, ANN have been widely used in machining due to their high predictive accuracy. Liman [15] employed the Response Surface Methodology (RSM) and ANN to predict surface roughness in UPM of polymer materials for contact lenses, demonstrating the importance of advanced modeling techniques in surface roughness prediction and control.

In smart manufacturing, various optimization algorithms are employed, including evolutionary algorithms (EA), swarm intelligence (SA) algorithms, convolutional neural networks (CNN), Q-learning, fuzzy logic, support vector machines (SVM), long short-term memory (LSTM), random forests (RF), backpropagation networks (BP), and K-nearest neighbor (KNN). Among these, the ABC algorithm, classified under SA, is an optimization algorithm inspired by the intelligent foraging behavior of honeybee colonies. Roy in [16] explored the integration of the genetic algorithm (GA) with ABC to solve the Green Four-Dimensional Traveling Salesman Problem (4DTSP). This approach optimized profitability in green manufacturing systems while effectively handling both discrete and continuous variables in logistics and resource management.

This paper focuses on developing a predictive model and optimizing surface roughness based on cutting parameters in the UPT of Al6061 spherical surfaces. Optimizing surface quality is crucial, particularly in high-precision applications such as optical systems, mold fabrication, and ultra-precision mechanical joints, where surface roughness plays a key role in ensuring operational performance. Experimental data from 30 experiments were used to analyze the interaction between cutting parameters and to develop an ANN model for predicting surface quality. Additionally, the ABC algorithm effectively handled complex solution spaces and was employed to identify optimal machining conditions, ensuring the required surface roughness while improving machining efficiency.

2. Research Content

2.1. ANN Model and ABC Algorithm

ANN has been widely utilized in research [13-15] due to its high prediction accuracy, while ABC is an intelligent optimization algorithm capable of efficiently searching for solutions in multidimensional spaces. The combination of these two methods enables highly accurate predictions of optimal outcomes in experimental models in general and SPDT machining conditions in particular. This integration helps reduce experimental machining time and enhances the quality of machined aparts.

2.1.1. ANN model

An ANN is a nonlinear mapping system inspired by the functions of the human brain. It consists of three layers (Fig. 1): the input layer, the hidden layer, and the output layer, each composed of one or more neurons, forming the general structure of an ANN. Numerical values are fed into the network through the neurons of the input layer. In the surface roughness optimization problem, these input values correspond to spindle speed, feed rate, and depth of cut. Each neuron in the input layer receives a single input value, which is then propagated to the hidden layers.

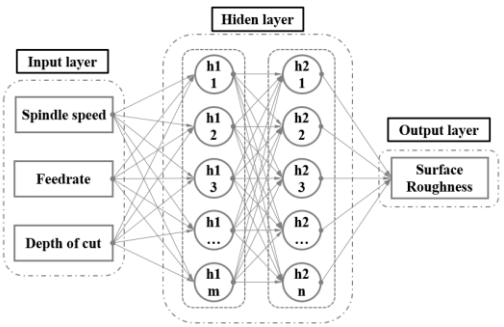

Fig. 1. Neural Network Structure

These layers are interconnected through synaptic weights, ensuring that every neuron in the hidden layer is connected to every neuron in the output layer, which in this case represents the predicted surface roughness value. The output layer provides numerical feedback values. Four key performance indicators: R^2, $MAPE$ [17], MSE, and $RMSE$ [18] are used to evaluate the accuracy of predictions by comparing the measured values (y_i) from N experiments with the predicted values ($\hat{y}_i$), thereby assessing the training quality and the model is fit.

2.1.2. ABC Algorithm

The ABC algorithm is one of the swarm intelligence algorithms inspired by the foraging behavior of honeybees. It was first introduced by Karaboga in [19]. This model simplifies the selection of food sources, which leads to the emergence of swarm intelligence in honeybee colonies. It consists of three main components: food sources, employed bees exploiting the sources, and unemployed bees, also known as scout bees. The model defines two primary behaviors: selecting employed bees for nectar sources and abandoning a food source. This model is illustrated in Fig. 2, while Table 1 summarizes the algorithm parameters.

Table 1. ABC Algorithm Parameters

N	Number of scout bees
A	Number of improved scout bees
B	Number of optimal scout bees
N_b	Number of worker bees following the optimal scout bees
N_a	Number of worker bees following the improved scout bees
H	Initial size of the neighborhood region
R	Neighborhood shrinking factor
T	Iteration limit before abandoning a site
D	Algorithm stopping criteria

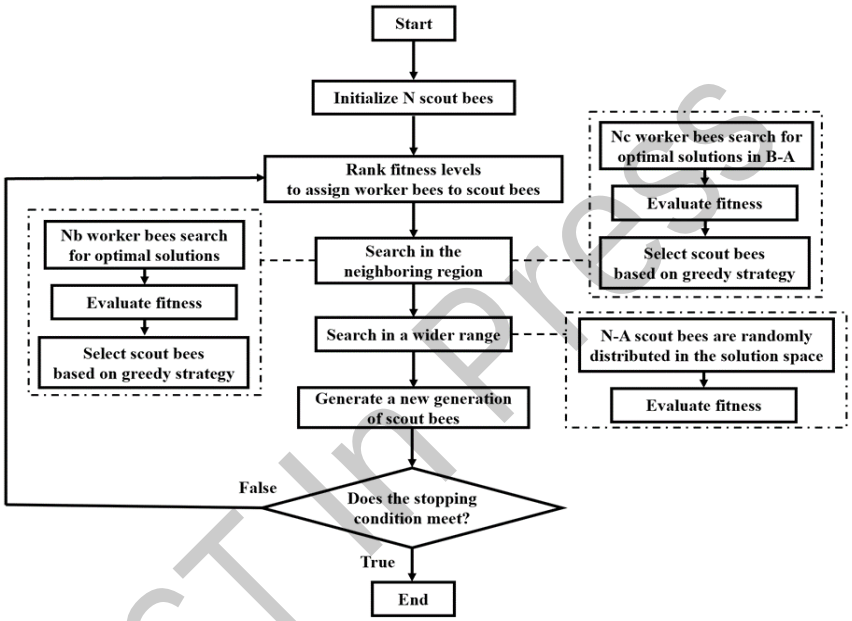

Fig. 2. ABC algorithm flowchart

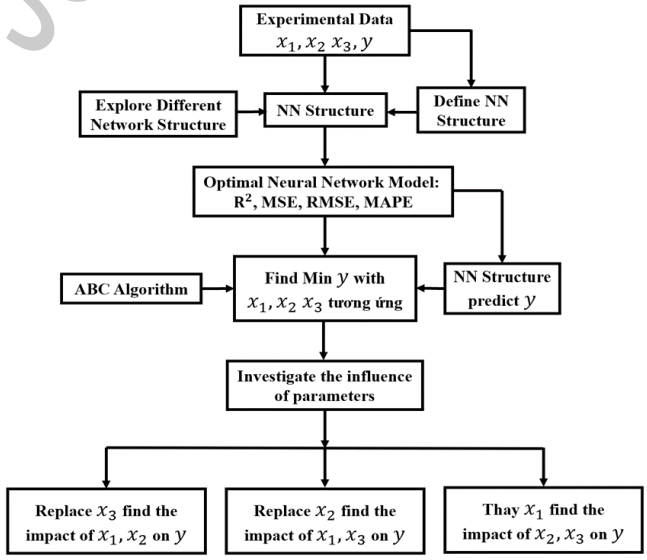

Fig. 3. Diagram of the ANN prediction model combined with the ABC optimization algorith

2.1.3. Building a predictive ANN model combined with the ABC optimization algorithm

The steps for integrating the ANN prediction model with the ABC optimization algorithm are illustrated in Fig. 3:

Step 1: Collect experimental data with input x_1, x_2, x_3 and output variables.

Step 2: Examine ANN structures: Test different ANN configurations (number of hidden layers, number of neurons per layer, activation functions, etc.). Define the ANN structure by selecting a specific network configuration based on the evaluation results.

Step 3: Select the best ANN model for predicting values based on the criteria: $R^2, MAPE, MSE$ and $RMSE$.

Step 4: Use the ABC algorithm to find the optimal Min value corresponding to x_1, x_2, x_3.

Step 5: Analyze each pair of variables to evaluate the impact of parameters on Y.

2.2. Establishing the Experimental Setup

The experiments were conducted on the Nanoform® X diamond turning machine from Precitech, which uses two linear axes (X, Z) combined with a rotary axis (C) and supported by STS. The cutting tool used is a NN60R0635mWGC-MS0454 diamond tool, with specific parameters listed in Table 2, and the workpiece setup diagram is shown in Fig. 4.

The experimental workpiece is made of aluminum 6061, with dimensions Ø30 mm x 20 mm and a spherical radius of R19.5, which has been machined on a CNC lathe. The chemical composition of the workpiece is listed in Table 3. The experiment investigates the influence of cutting parameters with their value ranges shown in Table 4, including: spindle speed n (rev/min), feed rate (F - mm/min), and depth of cut (t - µm) on the surface roughness (R_a - nm).

Table 2. Parameters of the diamond turning tool

Number	Radius	Included Angle	Rake Angle	Primary Clearance	Cutting Height
477052	0.684 mm	60°	-25°	12°	7.475 mm

Table 3. Chemical composition of Al6061

Aluminum	Chemical composition (%)								
	Mg	Si	Fe	Cu	Cr	Zn	Ti	Mn	Al
6061	0.8-1.2	0.4-0.8	0.7	0.15-0.4	0.04-0.35	0.25	0.15	0.15	Balance

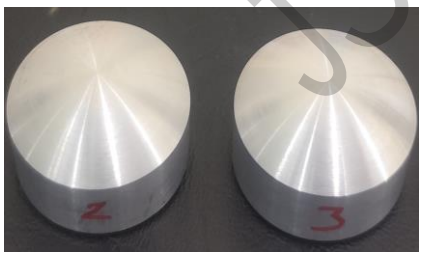

(a) Workpiece

(b) Diamond turning tool

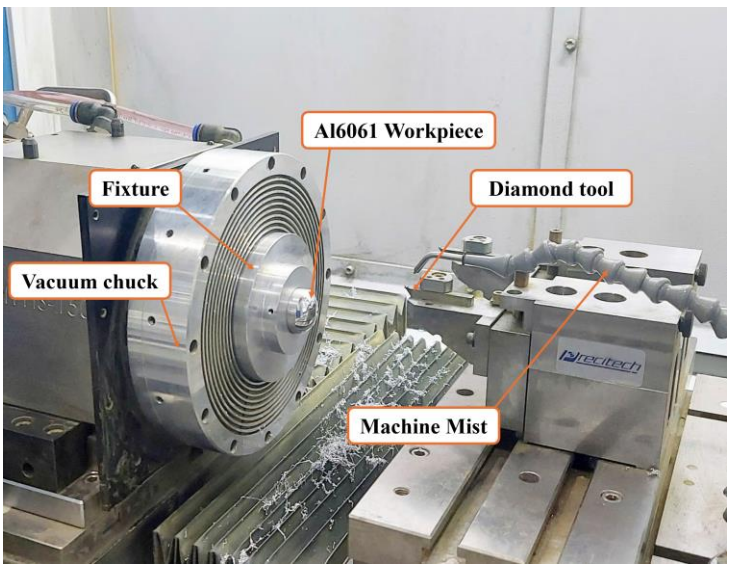

(c) Experimental system

Fig. 4. Diagram of the Workpiece Setup.

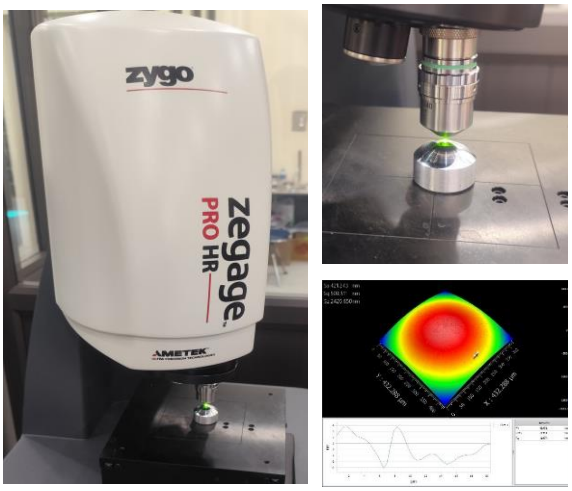

Fig. 5. Measuring surface roughness with Zegage HR interferometer

Table 4. Restrict experimental parameter range

Technology parameters	N (rev/min)	F (mm/min)	t (μm)
Corresponding variables	x_1	x_2	x_3
Low level $x_i = -1$	1000	5	2
Basic level $x_i = 0$	1500	15	5
High level $x_i = +1$	2000	25	8
Min value	823	1	1
Max value	2177	29	9

Table 5. Surface roughness measurements and machining conditions for 30 experiments

No.	n (rev/min)	F (mm/min)	t (μm)	Ra (nm)	No.	n (rev/min)	F (mm/min)	t (μm)	Ra (nm)
1	1000	5	5	4.61	16	1000	5	2	5.61
2	2000	5	5	4.05	17	2000	5	2	4.43
3	1000	25	5	6.29	18	1000	25	2	4.22
4	2000	25	5	2.09	19	2000	25	2	4.11
5	1000	15	2	2	20	1000	5	8	2.23
6	2000	15	2	4.85	21	2000	5	8	2.96
7	1000	15	8	6.62	22	1000	25	8	6.13
8	2000	15	8	5.5	23	2000	25	8	6.77
9	1500	5	2	5.82	24	823	15	5	6.96
10	1500	25	2	6.99	25	2177	15	5	4.34
11	1500	5	8	3.59	26	1500	1	5	3.77
12	1500	25	8	5.82	27	1500	29	5	5.48
13	1500	15	5	7.46	28	1500	15	1	4.79
14	1500	15	5	8.38	29	1500	15	9	7.23
15	1500	15	5	8.23	30	2000	15	5	3.27

2.3. Computation Results and Discussion

2.3.1. ANN model building results

The ANN model has a neural network structure defined with parameters shown in Table 6.

Several ANN models were built with the first hidden layer having 4, 5, or 6 neurons and the second hidden layer having 9, 10, 11, or 12 neurons. Specifically, the models include (3-4-9-1), (3-5-9-1), (6-9), (3-5-10-1), (3-4-11-1), (3-5-11-1), (3-6-11-1), and (3-6-12-1). The model evaluation results are shown in Table 7.

In all 8 models, the R^2 values are all greater than 0.92, reaching 0.98 in the (3-5-10-1) model. This indicates that the predictive models fit the actual data very well. As for the accuracy indicators such as $MAPE, MSE$, and $RMSE$, they show the differences between the models. The bar charts in Fig. 6 compare the $MAPE, MSE$, and $RMSE$ values corresponding to those in Table 7.

Table 6. Structure and computation results of the indicators: R^2, MSE, and $MAPE$

No.	ANN Model Parameters	Value
1	Number of input layer variables	3
2	Number of output layer variables	1
3	Number of neurons in the first hidden layer	Table 7
4	Number of neurons in the second hidden layer	Table 7
5	Data split ratio: Training / Validation / Testing	80%/10%/10%
6	Number of experiments	30
7	Transfer function	Poslin
8	Training function	traingd
9	Maximum number of epochs to train	10000
10	Fitness function	*MSE*
11	Learning rate	0.01
12	Momentum constant	0.9
13	Maximum allowable runs when the network fails to improve	6

Table 7. Networks structure (NS) and computation values for indicators R^2, MSE, $RMSE$, and $MAPE$.

NS	R^2			*MSE*			*MAPE (%)*			*RMSE*		
	Train	**Test**	**All data**	**Train**	**Test**	**All data**	**Train**	**Test**	**All data**	**Train**	**Test**	**All data**
4-9	0.94	0.94	0.94	1.78	1.34	1.74	20.52	23.83	21.48	1.33	1.16	1.32
5-9	0.93	0.98	0.94	2.05	0.66	1.81	21.98	13.36	20.61	1.43	0.81	1.34
6-9	0.95	0.97	0.94	1.42	0.99	1.64	20.41	12.07	20.02	1.19	1.00	1.28
5-10	0.98	0.92	0.98	0.47	2.75	0.68	12.31	27.89	13.36	0.68	1.66	0.82
4-11	0.92	0.97	0.93	2.27	0.70	1.92	21.04	14.22	19.36	1.51	0.84	1.39
5-11	0.93	0.96	0.93	2.03	0.72	1.73	22.78	19.61	20.96	1.13	0.85	1.31
6-11	0.94	0.99	0.95	1.77	0.21	1.45	20.54	9.41	18.03	1.33	0.46	1.21
6-12	0.95	0.99	0.96	1.29	0.21	1.06	16.34	5.19	13.93	1.13	0.46	1.03

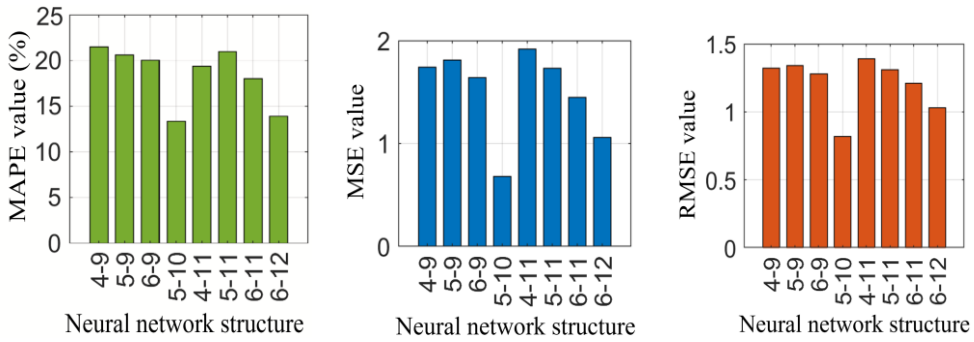

Fig. 6. $MAPE$, MSE, and $RMSE$ values corresponding to the structure ratios

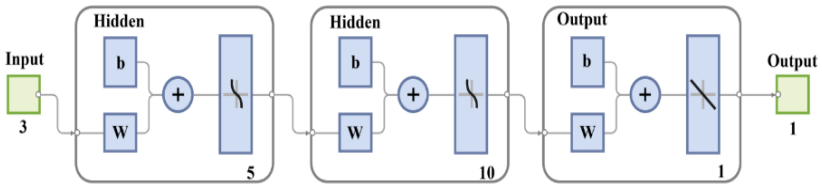

Fig. 7. Illustration of the 3-5-10-1 network structure.

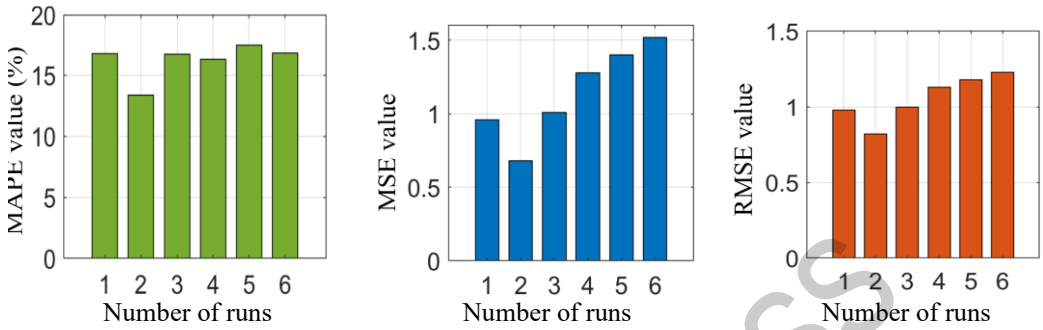

Fig. 8. *MAPE*, *MSE*, and *RMSE* values for the 3-5-10-1 structure over 6 runs.

Table 8. Number of runs (NOR) and Computation Results for R^2, *MSE*, *RMSE*, and *MAPE*.

NOR	R^2			*MSE*			*MAPE (%)*			*RMSE*		
	Train	**Test**	**All data**	**Train**	**Test**	**All data**	**Train**	**Test**	**All data**	**Train**	**Test**	**All data**
1	0.97	0.99	0.97	0.95	0.28	0.96	16.91	9.73	16.80	0.97	0.53	0.98
2	0.98	0.92	0.98	0.47	2.75	0.68	12.31	27.89	13.36	0.68	1.66	0.82
3	0.97	0.86	0.96	0.82	3.29	1.01	15.43	37.41	16.79	0.90	1.81	1.00
4	0.94	0.99	0.95	1.52	0.14	1.28	17.29	7.98	16.36	1.23	0.37	1.13
5	0.94	0.98	0.95	1.64	0.74	1.40	19.36	10.74	17.52	1.28	0.86	1.18
6	0.94	0.96	0.95	1.66	1.62	1.52	17.24	16.98	16.87	1.29	1.27	1.23

In the models above, the (5-10) model achieves the highest R^2 value and the lowest *MAPE*, *MSE*, and *RMSE*, demonstrating its superior prediction accuracy. The network structure 3-5-10-1 is shown in Fig. 7.

Each time the network is trained, the datasets for "Training," "Validation," and "Test" are randomly selected at the respective ratios of 80%:10%:10%. This results in different outcomes with each activation, reflecting the objectivity of the network construction and selection process. The 3-5-10-1 structure was run six consecutive times to identify the optimal dataset, and the survey results are presented in Table 8.

Based on the results in Table 8 and the depiction in Fig. 6, the (3-5-10-1) model in the second run achieved the highest R^2 value of 0.98 and the lowest values for *MAPE* (13.36%), *MSE* (0.68), and *RMSE* (0.82) compared to the other runs. The results from this run were subsequently used for ABC optimization.

2.3.2. Optimization results via the ABC algorithm

The ABC algorithm is configured with input parameters as shown in Table 9, which include 100 scout bees (initial solution count) and the optimization of 3 input variables [x_1, x_2, x_3] within the range from [823, 1, 1] to [2177, 29, 9]. The objective function is the pre-trained neural network with a (3-5-10-1) structure, with a maximum of 1000 evaluations and a failure limit of 300 per solution. These parameters are optimized to ensure rapid convergence and high accuracy.

Table 9. Input parameters (P) of the ABC algorithm.

P	Meaning	Value
N	Number of scout bees	100
B	Number of optimal scout bees	3
T	Iteration limit before abandoning a site	300
H	Initial size of the neighborhood region	
	Lower Limit	[823, 1, 1]
	Upper Limit	[2177, 29, 9]
D	Algorithm stopping criteria	Model ANN (3-5-10-1)

Table 10. Optimal results of the ABC algorithm runs

Number of runs	x_1	x_2	x_3	Ra
1	**823**	**13**	**1**	**0.76**
2	**823**	**13**	**1**	**0.76**
3	823	13	1	0.84
4	823	14	1	0.93
5	823	13	1	0.80
6	823	12	1	0.78
7	823	13	1	0.78
8	823	13	1	0.78
9	**823**	**13**	**1**	**0.76**
10	823	13	1	0.79

Table 11. Experimental results with optimal cutting conditions

No.exp	$R_a^{\exp}$ (nm)	R_a^{pred} (nm)	Error (%)
1	0.761	0.76	0.13
2	0.763	0.76	0.39
3	0.762	0.76	0.26

The ABC algorithm relies on random factors in initialization, search, and solution selection, so the optimal results vary with each run. Specifically, in this problem, the optimal surface roughness corresponding to the determined values of the three input variables over 10 consecutive runs is presented in Table 10. Based on these results, in runs 1, 2, and 9, the optimal surface roughness achieved the lowest value of 0.76 nm with the following cutting conditions: a spindle speed of *823 rev/min*, a feed rate of *13 mm/min*, and a depth of cut of *1 μm*.

Machining of the spherical surface was carried out using SPDT with the following cutting conditions: a spindle speed of *823 rpm*, a feed rate of *13 mm/min*, and a depth of cut of *1 μm*. The results from three experimental measurements of surface roughness ($R_a^{\exp}$, nm) are presented in Table 11. When these values are compared with the optimal surface roughness predicted by the ABC algorithm (R_a^{pred}, nm), the percentage error between the predicted and experimental values is less than 1%, demonstrating the high accuracy of the predictive model.

2.3.3. Results of factors influence analysis

Based on the optimal surface roughness of 0.76 nm, the influence of input variable pairs on the objective function was evaluated.

Effect of n and F on R_a (Fig. 7): value of R_a increases rapidly as spindle speed increases, reaching a maximum when the spindle speed is in the mid-range, and then decreases sharply as spindle speed continues to rise. When the spindle speed is below *1150 rev/min* and the feed rate is between *9 and 22 mm/min*, the surface roughness reaches a minimum value of less than *2nm*.

Influence of F and t on R_a (Fig. 8): when t is less than *4.5μm*, the surface roughness remains low; in this range, as the F increases, the surface roughness slightly decreases to a minimum, and then slightly increases as the feed rate continues to rise. Moreover, as the depth of cut increases, the surface roughness also increases. The minimum surface roughness, below *2 nm*, is achieved when the feed rate is between *9 and 22 mm/min* and the depth of cut is less than *2.5 μm*.

Influence of n and t on R_a (Fig. 9): as the spindle speed gradually increases up to *1800 rev/min* and the depth of cut gradually reaches *5.5 μm*, the surface roughness increases markedly from its minimum to maximum values. Then, as both spindle speed and depth of cut continue to rise, the surface roughness gradually decreases. When the spindle speed is below *1040 rev/min* and the depth of cut is less than *2 μm*, the surface roughness remains in the minimum range, with values below *2 nm*.

In general, value of R_a is predominantly influenced by spindle speed and a lesser extent by feed rate and cutting depth. A good surface finish with R_a less than *2 nm* is achieved when the spindle speed is below *1040 rev/min*, the feed rate is between *9 and 22 mm/min*, and the cutting depth is less than *2 μm*.

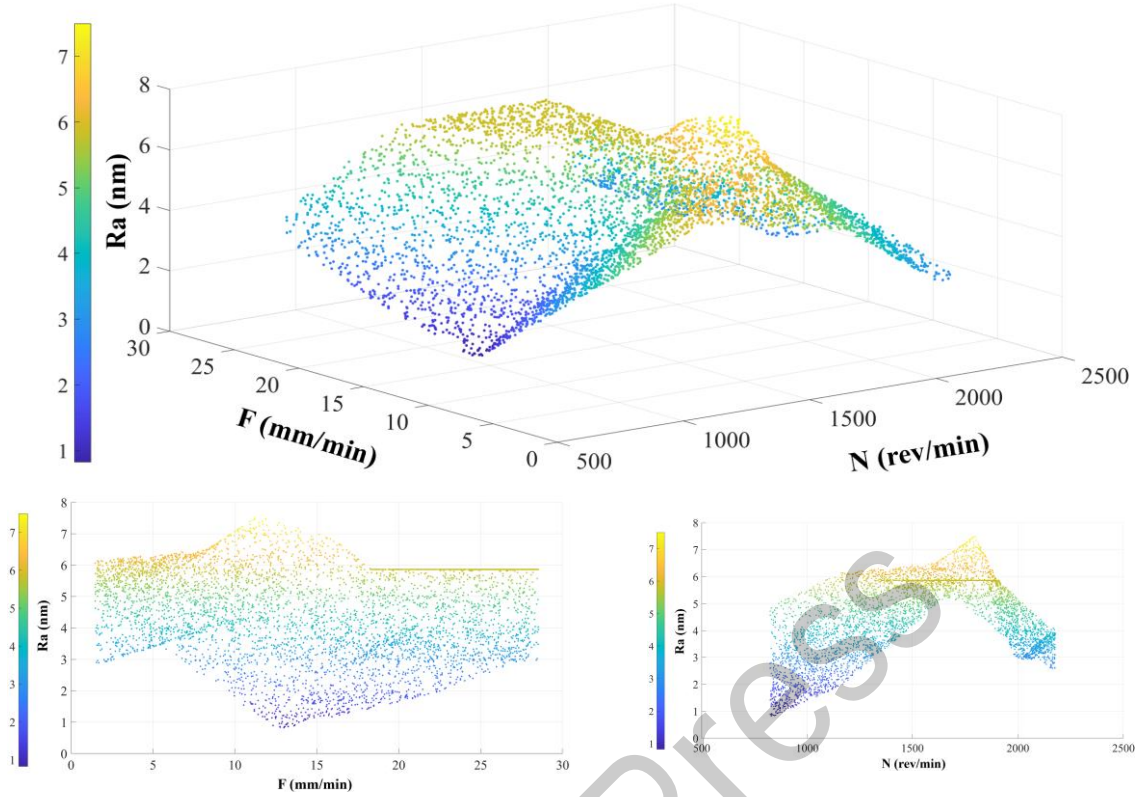

Fig. 7. Influence of n and F on R_a

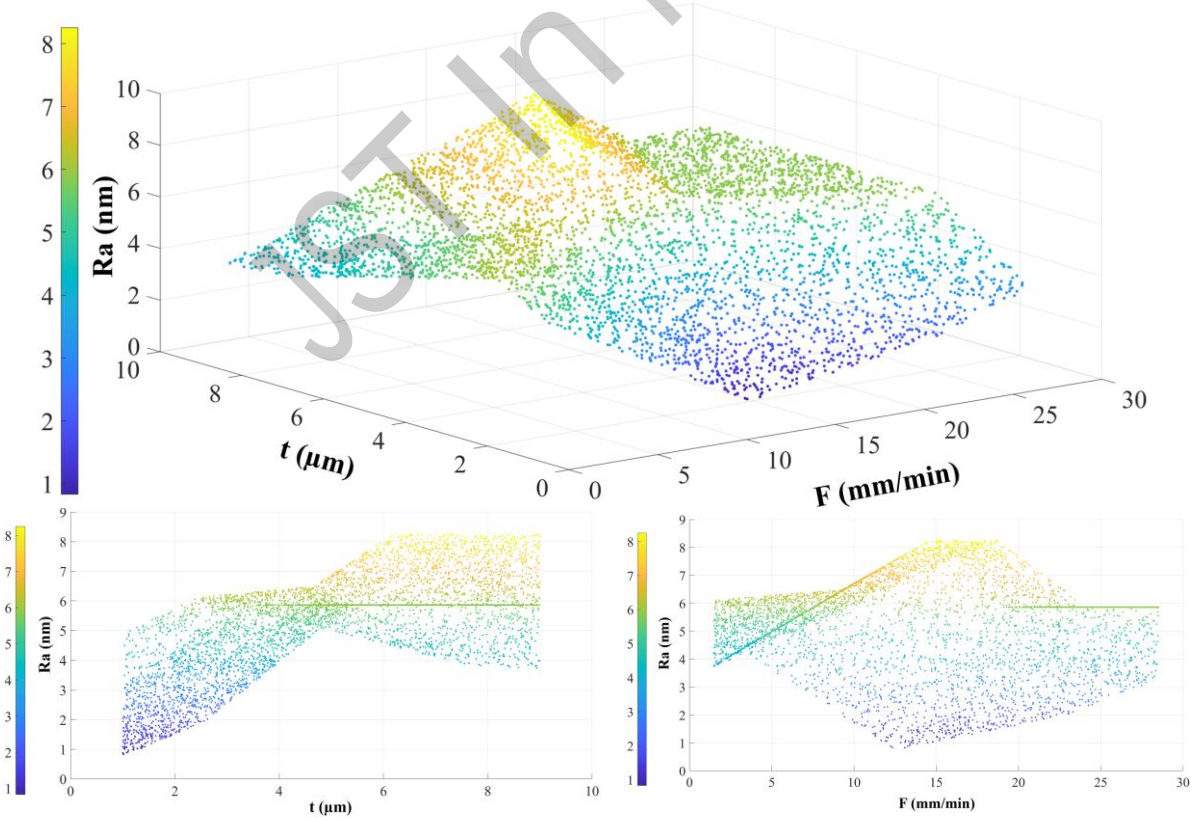

Fig. 8. Influence of F and t on R_a

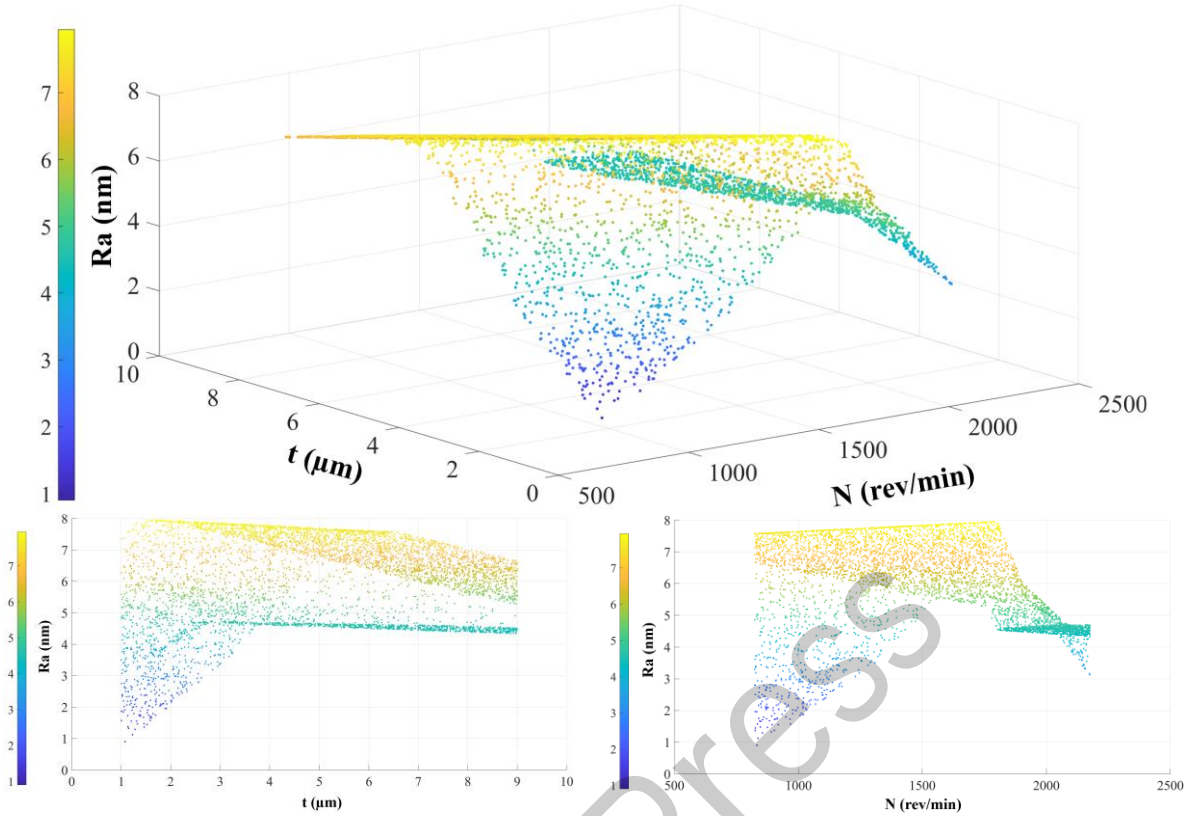

Fig. 9. Influence of n and t on R_a

3. Conclusion

In this paper, an ANN combined with the ABC algorithm is applied to predict and optimize surface roughness in the spherical surface machining process by SPDT for Al6061 material. The ANN is used to model the nonlinear relationship between cutting parameters (n, F, t) and R_a, while the ABC algorithm helps optimize the ANN model parameters to enhance prediction accuracy. With 30 experiments and the optimal ANN structure (3-5-10-1), the study achieved high reliability with an R^2 of 0.98 and performance metrics of *MAPE* is 13.36%, *MSE* is 0.68, and *RMSE* is 0.82. Based on the ABC algorithm, the optimal surface roughness was determined to be as low as *0.76nm* under the cutting conditions of a spindle speed of *823 rev/min*, a feed rate of *13 mm/min*, and a depth of cut of *1μm*. Furthermore, the study results indicate that cutting parameters such as spindle speed, feed rate and depth of cut significantly affect the surface roughness of Al6061, with spindle speed having the greatest influence. This research provides important insights into modeling and optimizing cutting parameters in ultra-precision turning of Al6061, and the approach can also be extended to other quality factors, such as dimensional error or surface form, as well as to other materials and machining processes for aspherical and diffractive surfaces.

References

[1] Z. Xu, T. Zhu, F. L. Luo, B. Zhang, H. Poon, and W. S. Yip, A review: insight into smart and sustainable ultra-precision machining augmented by intelligent IoT, Journal of Manufacturing Systems, vol. 74, pp. 233-251, Jun. 2024. https://doi.org/10.1016/j.jmsy.2024.03.008

[2] A. Gupta, A. Saini, N. Khatri, and A. Juyal, Review of single-point diamond turning process on IR optical materials, Materials Today: Proceedings, vol. 69, pp. 435-440, 2022. https://doi.org/10.1016/j.matpr.2022.09.073

[3] W. Huang and J. Yan, Mechanisms of tool-workpiece interaction in ultraprecision DT of single-crystal SiC for curved microstructures, International Journal of Machine Tools and Manufacture, vol. 191, pp. 104063, Oct. 2023. https://doi.org/10.1016/j.ijmachtools.2023.104063

[4] Z. Liu, J. Wang, R. Leng, *et al*., Impact of mirror local defects on system scattering in telescopes, Results Physics, vol.56, pp. 107265, Jan. 2024. https://doi.org/10.1016/j.rinp.2023.107265

[5] W. Gao, S. Ibaraki, M. A. Donmez, *et al*., Machine tool calibration: measurement, modeling, and compensation of machine tool errors, International Journal of Machine Tools Manufacture, vol. 187, pp. 104017, Apr. 2023. https://doi.org/10.1016/j.ijmachtools.2023.104017

[6] K. A. E. Hossein and O. A. Olufayo, Diamond machining of rapidly solidified aluminium for optical mould inserts, Procedia Materials Science, vol. 6, pp. 1077–1082, 2014. https://doi.org/10.1016/j.mspro.2014.07.178

[7] M. Mukaida and J. Yan, Ductile machining of single-crystal silicon for microlens arrays by ultraprecision diamond turning using a slow tool servo, International Journal of Machine Tools Manufacture, vol. 115, pp. 2-14, Apr. 2017. https://doi.org/10.1016/j.ijmachtools.2016.11.004

[8] M. Mia and N. R. Dhar, Prediction of surface roughness in hard turning under high pressure coolant using artificial neural network, Measurement, vol. 92, pp. 464–474, Oct. 2016. https://doi.org/10.1016/j.measurement.2016.06.04

[9] M. M. Liman, K. A. E. Hossein, and P. B. Odedeyi, Modeling and prediction of surface roughness in ultra-high precision diamond turning of contact lens polymer using RSM and ANN methods, Materials Science Forum, vol. 928, pp. 139–143, Aug. 2018. https://doi.org/10.4028/www.scientific.net/MSF.928.139

[10] G. S. Khan, Characterization of surface roughness and shape deviations of aspheric surfaces, Ph.D. dissertation, 2008.

[11] S. J. Zhang, S. To, S. J. Wang, and Z. W. Zhu, A review of surface roughness generation in ultra-precision machining, International Journal of Machine Tools Manufacture, vol. 91, pp. 76–95, Apr. 2015. https://doi.org/10.1016/j.ijmachtools.2015.02.001

[12] S. Hatefi and K. A. E. Hossein, Review of single-point diamond turning process in terms of ultra-precision optical surface roughness, The International Journal of Advanced Manufacturing Technology, vol. 106, pp. 2167-2187, Dec. 2019. https://doi.org/10.1007/s00170-019-04700-3

[13] L. H. Li, N. H. Yu, C. Y. Chan, and W. B. Lee, Al6061 surface roughness and optical reflectance when machined by single point diamond turning at a low feed rate, PLoS ONE 13(4): e0195083, Apr. 2018. https://doi.org/10.1371/journal.pone.0195083

[14] W. Gao, H. Haitjema, F. Z. Fang, *et al*., On-machine and in-process surface metrology for precision manufacturing, CIRP Annals, vol. 68, iss. 2, pp. 843–866, 2019. https://doi.org/10.1016/j.cirp.2019.05.005

[15] R. J. Bensingh, R. Machavaram, S. R. Boopathy, and C. Jebaraj, Injection molding process optimization of a bi-aspheric lens using hybrid artificial neural networks (ANNs) and particle swarm optimization (PSO), Measurement, vol. 134, pp. 359–374, Feb. 2019. https://doi.org/10.1016/j.measurement.2018.10.066

[16] S. Roy, A. Khanra, S. Maity, R. K. Pal, and M. Maiti, GA-ABC hybridization for profit maximization of green 4DTSPs with discrete and continuous variables, Engineering Applications of Artificial Intelligence, vol. 123, part B, pp. 106293, Aug. 2023. https://doi.org/10.1016/j.engappai.2023.106293

[17] M. R. Sankar, S. Saxena, S. R. Banik, I. M. Iqbal, R. Nath, L. J. Bora, K. K. Gajrani., Experimental study and artificial neural network modeling of machining with minimum quantity cutting fluid, Materials Today: Proceedings, vol. 18, pp. 4921–4931, 2019. https://doi.org/10.1016/j.matpr.2019.07.484

[18] L. Fan, Y. Ren, M. Tan, B. Wu, and L. Gao, GA-BP neural network-based nonlinear regression model for machining errors of compressor blades, Aerospace Science Technology, vol. 151, pp. 109256, Aug. 2024. https://doi.org/10.1016/j.ast.2024.109256

[19] D. Karaboga, An idea based on honey bee swarm for numerical optimization, Tech. Rep. TR-06, Oct. 2005.

[20] M. Aamir, M. T. Rad, K. Giasin, and A. Vafadar, Machinability of Al2024, Al6061, and Al5083 alloys using multi-hole simultaneous drilling approach, Journal of Materials Research Technology, vol. 9, iss. 5, pp. 10991-11002, Sep-Oct. 2020.